ACS APPLIED MATERIALS & INTERFACES

Research Article

www.acsami.org

Thickness and Microdomain Orientation of Asymmetric PS-*b*-PMMA Block Copolymer Films Inside Periodic Gratings

Federico Ferrarese Lupi,*[,†] Giulia Aprile,[‡,§] Tommaso Jacopo Giammaria,[†,§] Gabriele Seguini,[†] Giampaolo Zuccheri,[∥] Natascia De Leo,[‡] Luca Boarino,[‡] Michele Laus,[§] and Michele Perego[†]

[†]Laboratorio MDM, IMM-CNR, Via C. Olivetti 2, 20864 Agrate Brianza, Italy

[‡]NanoFacility Piemonte, Istituto Nazionale Ricerca Metrologica, Strada delle Cacce 91, 10135 Torino, Italy

[§]Dipartimento di Scienze e Innovazione Tecnologica (DISIT), Università del Piemonte Orientale "A. Avogadro", INSTM, UdR Alessandria, Viale T. Michel 11, 1512 Alessandria, Italy

[∥]Dipartimento di Farmacia e Biotecnologie, INSTM, Centro S3, CNR-Istituto Nanoscienze, Via Irnerio 48, Bologna 40126, Italy

S *Supporting Information*

ABSTRACT: The ordering process of asymmetric PS-*b*-PMMA block copolymers (BCPs) is investigated on flat SiO_2 surfaces and on topographically patterned substrates. The topographic patterns consist of periodic gratings of 10 trenches defined by conventional top-down approaches and subsequently neutralized using a P(S-*r*-MMA) random copolymer (RCP). When the ordering process is accomplished on a flat surface at a temperature ranging between 180 and 230 °C, cylindrical microdomains perpendicularly oriented with respect to the substrate are observed irrespective of annealing temperature. In contrast, when the ordering process occurs on topographically patterned substrates, different phenomena have to be considered. The simultaneous effect of the flow around the gratings and the BCP flux from the zone located between adjacent trenches (mesa) into the inner part of the trenches results in significant thickness variations of the confined BCP film. Therefore, the amount of BCP inside the trenches depends on the width of the mesa region, which acts as a BCP reservoir. Moreover, within each trench group, the BCP thickness progressively decreases from the external to the central trenches composing the periodic grating. The thickness variation of the BCP film within the trenches strongly affects the ordering process, ultimately leading to different orientations of the microdomains within the trenches. In particular, when the annealing temperature is 190 °C a precise confinement of the BCP within the trenches featuring a perpendicular cylinder morphology is observed. At higher temperatures, mixed or parallel orientations of the microdomains are obtained depending on the width of the trenches in the periodic grating.

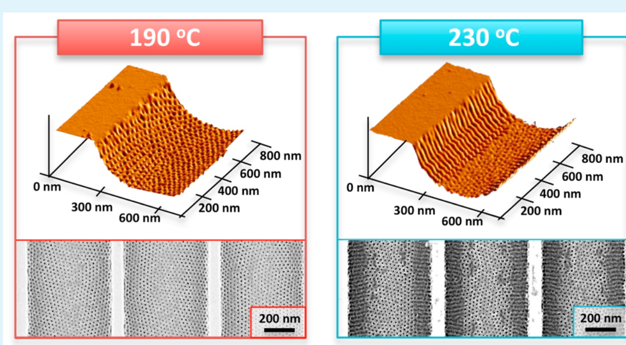

KEYWORDS: *PS-b-PMMA, self-assembly, trench, thin film, rapid thermal annealing, graphoepitaxy*

INTRODUCTION

Because of the intrinsic limits of optical lithography, the microelectronic industry is facing several technological and fundamental bottlenecks to produce nanoscopic structures with typical feature sizes below 15 nm. The identification of the most reliable and cheap technology to obtain nanostructures approaching the 10 nm node, as defined by the International Technology Roadmap for Semiconductors (ITRS),[1] is still an open issue. Block copolymer (BCP)-based nanolithography represents an interesting option.[2,3]

BCPs are a particular class of macromolecules ideally produced by joining two or more chemically distinct and thermodynamically incompatible polymeric blocks. These macromolecules are able to self-assemble in a variety of periodic morphologies (i.e., cylinders, lamellae, spheres, and gyroids) with characteristic lengths at the nanometer scale. The registration of the BCP periodic microdomains in a predefined location of the substrate is a prerequisite for the integration of these materials into a photolithographic process flow and requires the control of the in-plane positioning of the periodic features in the polymeric films. Several methods were proposed to register the BCP microdomains to the substrate surface, including chemical patterning of the substrate[4,5] as well as soft[6,7] and hard graphoepitaxy techniques.[8,9] In particular, hard graphoepitaxy refers to the fabrication of topographic structures on the substrate to confine the BCP film and direct the self-assembly process.[10−12] By topographically sectoring a surface with standard lithographic processes, addressable arrays of spherical,[13,14] cylindrical,[15,16] or lamellar[17−19] elements can be registered with the underlying substrate featuring a high degree

Received: August 3, 2015
Accepted: October 6, 2015
Published: October 6, 2015

 © 2015 American Chemical Society

DOI: 10.1021/acsami.5b07127
ACS Appl. Mater. Interfaces 2015, 7, 23615−23622

of lateral order and correlation in the *xy* plane. However, few studies[20,21] are focused on the arrangement and ordering characteristics of the BCP features as a function of the thickness of the confined polymeric film. Nevertheless, the flow of BCP into the trenches from the zone adjacent to the periodic grating[11] (also known as the backwash effect) leads to significant variations of the film thickness within the trenches, affecting microdomain orientation and lateral ordering of the BCP template. In particular, cooperative ordering mechanisms, such as the orientation flipping of the cylindrical domains from parallel to perpendicular with respect to the substrate,[22,23] need be thoroughly investigated and understood to exploit BCP-based lithography in large-scale production.

The aim of this manuscript is to analyze the flow of the polymeric film into random copolymer (RCP)-neutralized periodic structures topographically defined into a SiO_2 substrate and to correlate it with the final thickness of the confined polymeric film upon annealing. The orientation of the microdomains in cylinder-forming PS-*b*-PMMA films (M_n = 54 kg·mol^{-1}, styrene unit fraction of 0.71) confined inside gratings of 10 trenches is investigated as a function of the geometrical parameters of the trenches at different annealing temperatures ranging from 180 to 230 °C.

EXPERIMENTAL SECTION

Grating Fabrication. Periodic gratings of 10 trenches, with different widths (W) between 70 and 600 nm and located at variable distances (d) of 100, 200, 300, and 400 nm, were fabricated by e-beam lithography in 100 nm thick SiO_2 films thermally grown on Si(100) substrates (Figure 1). The depth of the trenches was fixed at 90 nm.

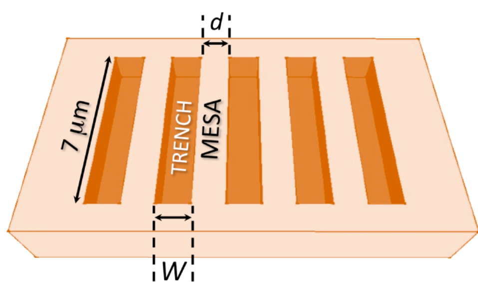

Figure 1. Scheme of the periodic gratings.

Nanolithography of the trenches was carried out by a FEI Quanta 3D dual-beam ESEM-FEG equipped with NPGS by J.C. Nabity Systems on PMMA resist at 30 kV after an accurate exposure dose test with a 6 pA current. The resist was developed in a standard MIBK/IPA 1:3 solution for 60 s, stopped in IPA for 20 s, and rinsed in deionized (DI) water for 20 s. Reactive ion etching (RIE) was carried out in a Plasmalab 80 Plus at a pressure of 40 mTorr with a gas mixture of CHF_3 (60 sccm) and Ar (25 sccm). The SiO_2 trench depth of 90 nm was controlled by setting the power of the RF generator to 120 W and the bias voltage to 340 V, for an overall etching time of 240 s. The final depth of the periodic structures after the RIE process is independent of the trench width W, as observed in the AFM profiles reported in Figure S1.

Substrate Neutralization. To neutralize the substrate, a solution with 18 mg of P(S-*r*-MMA) RCP (styrene fraction = 0.62, M_n = 1.7 kg·mol^{-1}, and PDI = 1.19) in 2 mL of toluene was prepared in ultrasonic bath. The −OH terminations of the RCP were used to promote the grafting to the prepatterned silicon oxide substrate. The P(S-*r*-MMA) solution was spun for 30 s at 3000 rpm. The 30 nm thick RCP film provides a complete cover of the periodic gratings with a RCP film, as reported in Figure S2. To induce the grafting of the RCP, the samples were annealed in rapid thermal processing (RTP) machine for 60 s at 310 °C.[24] The ungrafted chains were removed with a 300 s sonication step in a toluene bath. The thickness of the resulting grafted layer was ~2 nm as detected by ellipsometry. In this particular combination of spinning parameters, RCP thickness and trench depth as well as the sidewalls of the trenches are neutralized by the RCP.[23]

Block Copolymer Deposition. The asymmetric PS-*b*-PMMA block copolymer marked B54, with styrene unit fraction of 0.71, M_n = 54 kg·mol^{-1}, and PDI = 1.07, was purchased from Polymer Source Inc. and used without further purification. A solution of PS-*b*-PMMA in toluene was prepared (18 mg in 2 mL) and spun for 30 s at 3000 rpm to obtain an ~30 nm thick layer on the flat surface. Block copolymer ordering was carried out by RTP treating the sample in N_2 atmosphere at annealing temperatures T_a between 180 and 230 °C. In this temperature range, the dependence of χ on the annealing temperature is quite weak for PS-*b*-PMMA block copolymers.[25] The annealing time was set at t_a = 900 s. On the flat surface of the sample, the domain period of such cylindrical features is length L_0 = 28.8 nm and diameter d = 13 nm.[26]

Morphology Characterization. The surface morphology of the BCP samples was studied by scanning electron microscopy (SEM) using a Zeiss InLens system and by atomic force microscopy (AFM) with a Multimode 8 NanoScope V with a J-type piezo scanner (Bruker). Imaging was carried out at ambient temperature and humidity in peak-force tapping and in tapping-mode with ScanAsyst-air (Bruker) and NSC15/AIBS (MikroMasch) probes, respectively, acquiring simultaneously both the topography and the phase signals. To enhance the contrast during the acquisition of the SEM images, the PMMA cylinders were selectively removed. A 900 s exposure to UV radiation (5 mW·cm^{-2}, λ = 253.7 nm) allows degradation of PMMA and cross-linking of the PS matrix. The degraded PMMA material was then removed by immersion in acetic acid for 300 s. The samples were

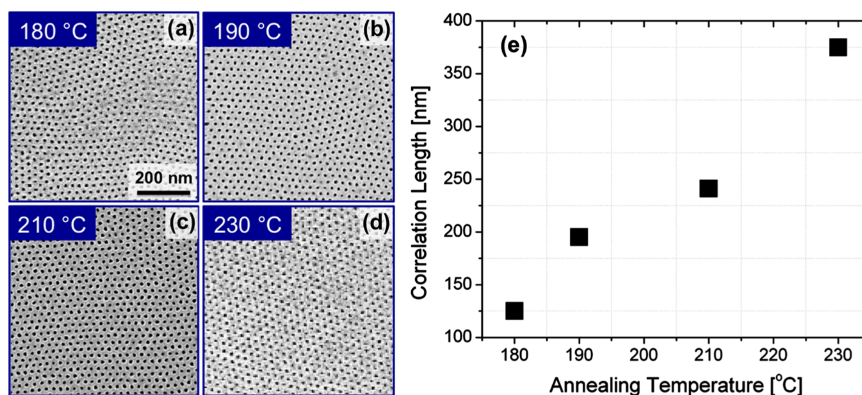

Figure 2. (a−d) SEM micrographs of B54 ordered on the flat surface at different annealing temperatures. (e) Correlation length ξ as a function of the annealing temperature for B54.

DOI: 10.1021/acsami.5b07127
ACS Appl. Mater. Interfaces 2015, 7, 23615−23622

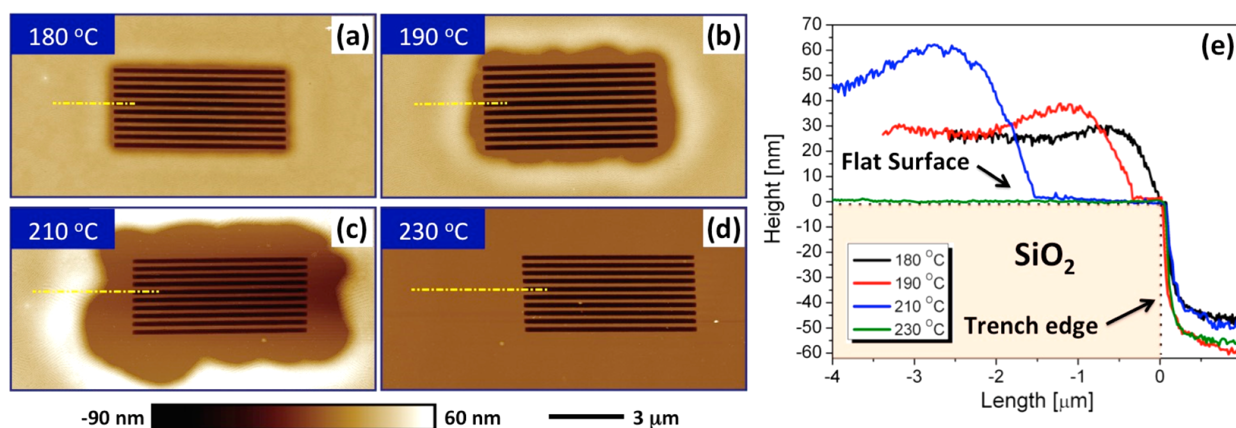

Figure 3. AFM top-view images reporting the effect of the annealing temperature on the BCP film in the region near the grating, for (a) T_a = 180 °C, (b) 190 °C, (c) 210 °C, and (d) 230 °C. (e) AFM height profiles measured across the yellow dashed lines of a−d, describing the height profiles of the BCP rims at the distinct annealing temperatures.

subsequently rinsed in DI water. Finally, O_2 plasma treatments were carried out to remove the residual PMMA and the RCP at the bottom of the pores.

RESULTS AND DISCUSSION

BCP Ordering on Flat Surfaces. To characterize the dependence of the correlation length ξ on the annealing temperature T_a on the flat surface, a first set of samples was prepared by spin coating ∼30 nm thick B54 films on properly neutralized SiO_2 surfaces. The ordering process was carried out by heating at 18 °C/s^{-1} to a temperature between 180 and 230 °C and maintaining the sample at this temperature for t_a = 900 s. This particular t_a was chosen as a trade-off between the technological request of a short processing time and the necessity to reach a long-range order degree within the self-assembled domains. As discussed in our previous studies, when operating at high temperatures, this particular annealing time leads to the formation of the equilibrium morphology.[27,28] Negligible evolution of the lateral order was reported to occur by further increasing the annealing time.

In Figure 2a−d are reported some representative SEM top-view images of the BCP template at different annealing temperatures. The formation of a homogeneous texture of hexagonally packed cylinders perpendicularly oriented with respect to the SiO_2 surface is observed over the entire sample, irrespective of the annealing temperature. However, when T_a is 230 °C, the occurrence of some disordered regions (not shown) suggests that the order−disorder transition temperature is close to 230 °C indicating that the processing window of accessible annealing temperatures for this specific BCP extends up to 230 °C. The ξ values were extracted from the SEM images according to the previously described method.[29,30] The ξ value for the sample annealed at T_a = 230 °C was extracted taking into account only the zones of the sample with the perpendicular PMMA cylinders. A monotonic increase in ξ is observed in BCP template as the annealing temperature increases, with correlation length values ranging from ξ = 120 nm for T_a = 180 °C to ξ = 375 nm for T_a = 230 °C. This progressive increase of the correlation length as a function of annealing temperature on flat surfaces is consistent with previously reported data for a BCP with M_n = 67 kg·mol^{-1}.[30] In this regard, it is worth noting that the two PS-*b*-PMMA BCPs exhibit different T_a values corresponding to the beginning of inhomogeneity appearance; the processing window of accessible T_a values for the B54 BCP is limited to 230 °C. This value is significantly lower than that in the case of the PS-*b*-PMMA BCP with M_n = 67 kg·mol^{-1}.[30]

Flow Mechanism into Periodic Trenches. The ordering mechanism of B54 BCP thin films within topographically defined structures was investigated as a function of the geometrical parameters of the periodic gratings, operating at T_a values comprised within the processing window identified on flat substrates. In Figure 3a−d are reported the AFM images taken of a representative group of gratings (W = 260 nm, d = 100 nm) after BCP deposition and treatment at different T_a. The AFM height profiles along the yellow dashed lines depicted in Figure 3a−d are shown in Figure 3e.

The AFM top-view images demonstrate that the annealing process induces a significant redistribution of the polymeric film in the region adjacent to the gratings. The BCP flows from the mesa into the trenches, emptying the area between the trenches. In the outer zone of the grating, the BCP film reflows farther away with respect to the periodic grating, forming a rim consisting in a local increase in the film thickness. This leaves the substrate surface exposed because of the so-called backwash effect.[11] The progression of the backwash, occurring along the short edge of the trenches at different annealing temperatures, is represented in the AFM height profiles shown in Figure 3e. At T_a = 180 °C, the BCP film extends continuously across the trenches, and an imperfect confinement is obtained. In contrast, when the samples are annealed at $T_a \geq$ 180 °C, the film fractures in correspondence to the trench edges. The exposed area of the substrate and the height of the rim progressively increase with T_a. At T_a = 230 °C, the formation of the rims is observed at a distance higher than 5 μm away from the periodic gratings (Figure S4). Interestingly, a few micrometers away from the rim, the film thickness stabilizes to h = 30 nm as with the flat surface.

Similar effects were previously reported for symmetric PS-*b*-PMMA deposited on a flat surface and annealed in vacuum at 170 °C for several hours.[31,32] For a BCP thickness of ∼30 nm, the authors observed the formation of rims corresponding to local discontinuities of the film. The formation of the rims and their dynamics is probably connected to the relaxation of molecular orientation previously induced by the spin-coating process and frozen at room temperature. Once the film is treated at high temperature and it breaks at the edge of the trenches, the stress is no longer counterbalanced, and the

relaxation of the molecular orientation causes a sliding of the film over the substrate surface. The entity of this sliding increases as the temperature increases because of the concomitant decrease of the friction coefficient. In turn, the higher the retraction distance and the temperature, the higher the rim height.

BCP Microdomain Orientation within Periodic Trenches. As already reported, BCP confinement within the trenches is a prerequisite in order to control their lateral ordering.[11] Defect-free PS-*b*-PMMA templates were obtained in perfectly confined thin BCP film,[23] whereas extended defects were observed in the case of partial confinement because of the interference between the ordering process in the trenches and that on the flat area surrounding the trenches.[11] For this reason, we restricted the processing window of the accessible temperature to the range of 190−230 °C, corresponding to the perfect confinement of the BCP film within the trenches. The orientation and lateral ordering of the BCP microdomains within the trenches was investigated in detail as a function of the geometrical parameters of the gratings at different T_a.

When the ordering of the BCP is carried out at 190 °C, a perpendicular orientation of the cylinders extending over the entire trench length occurs, irrespective of the trench width W (Figure 4a,d). However, an increase in the annealing temperature produces a substantial change in the orientation characteristics within the trenches. In particular, when the annealing is carried out at 210 °C, domains featuring perpendicular or parallel orientation with respect to the substrate coexist inside the trenches (Figure 4b,e). This effect is even more evident on increasing the temperature to 230 °C (Figure 4c,f). In addition, in the case of narrow trenches, the parallel cylinders cross the whole trench area (Figure 4b,c), whereas in wide trenches, a different domain arrangement is observed (Figure 4e,f) consisting of a central zone of perpendicular cylinders and two lateral areas symmetrically placed to the central zone, featuring cylinders in the parallel orientation to the substrate surface and perpendicularly oriented with respect to the long side of the trenches. This is due to the presence of RCP on the sidewalls of the trenches that induces the PMMA cylinders to orient themselves parallel to the substrate and perpendicular to the long sides of the trenches.

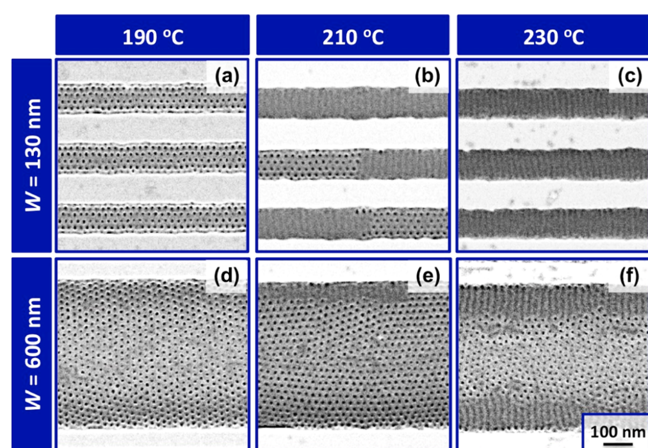

Figure 4. SEM images representing the surface morphology of BCP films confined inside a periodic structure with same mesa width d = 100 nm and variable trench width (a−c) W = 130 nm and (d−f) W = 600 nm, treated at T_a = 190, 210, and 230 °C.

A systematic analysis of SEM top-view images was carried out in order to quantitatively address this phenomenon and to correlate the orientation of the BCP microdomains with the processing conditions and geometrical parameters of the periodic gratings. In particular, Figure 5 reports the fraction of the internal area of the trenches with perpendicular cylinders as a function of the trench width W while still keeping the mesa width constant at d = 100 nm. Data are collected for different annealing temperatures corresponding to 190, 210, and 230 °C. At 190 °C, perpendicularly oriented cylinders are always observed irrespective of the trench width. In contrast, at 210 °C, the fraction of the perpendicularly oriented domains is zero when W is between 50 and 100 nm but suddenly increases as the trench width increases, reaching a plateaulike value of approximately 0.9 for W = 170 nm. It is worth noting that even in the case of large trenches (W > 200 nm) a small fraction of the area within the trenches is characterized by parallel orientation of the PMMA cylinders. At this temperature, perpendicular orientation of the microdomains with respect to the substrate cannot be achieved over the entire trench area. Finally, at 230 °C the fraction of perpendicularly oriented cylinders is 0 for W = 100 nm and then increases with increasing the trench width, reaching the maximum value of 0.5 corresponding to the widest trench (W = 600 nm).

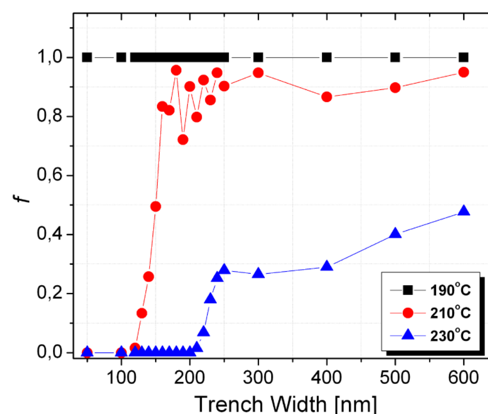

Figure 5. Fraction of the internal trench area containing perpendicular oriented cylinders (f) as a function of the trench width W for samples annealed at 190, 210, and 230 °C.

The film thickness and geometric boundary effects on the cylinder orientation at 190 and 230 °C are illustrated in Figure 6. In this figure is reported the AFM peak-force tapping analysis showing the organization of the BCP inside the trenches with respect to the height profile of the nanostructured BCP film. Note that in order to give an overall view of the topography among and within the trenches it was necessary to set different horizontal (μm) and vertical (nm) size scales. The AFM analysis was carried out inside a trench with W = 600 nm and d = 100 nm for a sample treated at T_a = 190 °C (Figure 6a−c) and T_a = 230 °C (Figure 6e−g) together with the thickness profile within this group of trenches (Figure 6d,h, respectively).

At T_a = 190 °C, in the longitudinal direction the orientation of the cylinders is perpendicular over the entire trenches. Conversely, at T_a = 230 °C, in the central zone of each trench annealed, the orientation of the cylinders is perpendicular, whereas near the sidewalls, only parallel cylinders are present.

DOI: 10.1021/acsami.5b07127
ACS Appl. Mater. Interfaces 2015, 7, 23615−23622

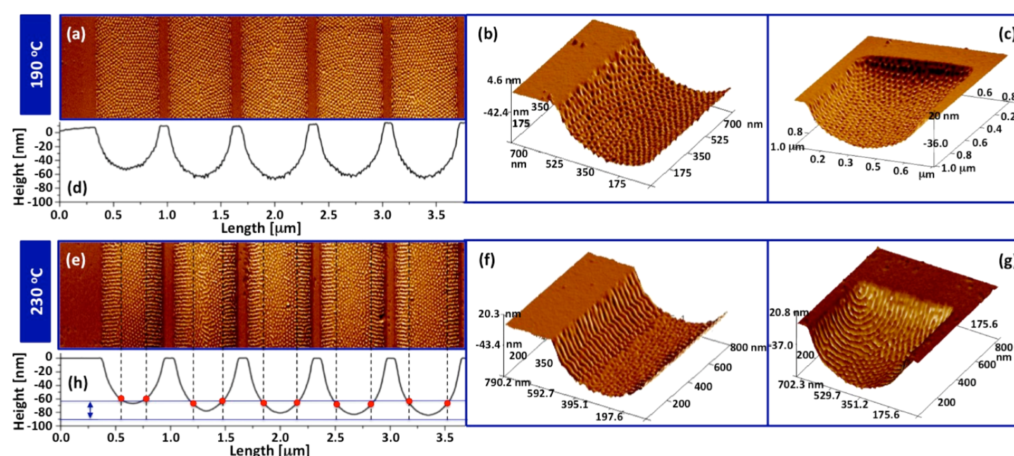

Figure 6. (a) AFM phase image for the sample annealed at T_a = 190 °C for t_a = 900 s and geometrical parameters W = 600 nm and d = 100 nm. The 3D perspective renderings of the film architecture inside the trenches in the central portion and close to the trench end are also reported in b and c, respectively. (d) AFM height profile across the trenches in a. (e) AFM phase image for the sample annealed at T_a = 230 °C for t_a = 900 s and geometrical parameters W = 600 nm and d = 100 nm showing the structuring across the trenches. The corresponding 3D perspective rendering of the film architecture inside the trenches treated at T_a = 230 °C are also reported: (f) in the central portion and (g) close to the trench end (texture mapping according to AFM phase data). (h) AFM height profiles across the trenches in e. The blue line indicates the thickness at which the orientation transition between parallel and perpendicular appears.

By tracing the lines delimiting the zones with different orientations (black dashed lines in Figure 6e) and referencing them with the AFM profiles (Figure 6h), it is clear that at 230 °C the perpendicular orientation can be obtained only for film thicknesses lower than 30 nm. Above this threshold thickness, the confined cylinders are arranged parallel to the neutral substrate. Because of the different thicknesses of the block copolymer layer within the various trenches, the width of the perpendicularly oriented area increases on from the center to the periphery of the grating. It is also interesting to observe that at T_a = 230 °C an abrupt change from perpendicular to parallel orientation is detected on moving from the inner trench region to the trench edges including the head region (Figure 6f,g). Here, the perspective plot informs on the 3D shape of the film, whereas the texture mapping of the rendering reports on the surface nanostructuring as better evident from the AFM phase data. Conversely, at 190 °C, the perpendicular orientation of the cylinders is observed also in proximity of the sidewalls (Figure 6b) or in the trench head region (Figure 6c) where the film thickness changes and peculiar boundary geometries are present.

Effect of Mesa Width on BCP Film Thickness and Microdomain Orientation. On the basis of the results reported in the previous sections, perpendicular orientation of the PS-*b*-PMMA microdomains within the trenches can be obtained by operating at 190 °C irrespective of W for a fixed distance between the trenches (d = 100 nm), yet according to collected data, a significant flow of polymeric material was observed moving from the mesa into the trenches. In view of the exploitation of this technology for lithographic application, it is necessary to consider that in real processes the distance between the different topographic features on the surface could be very different. Consequently the polymer flow from the mesa into the trenches could result in significant variations of the thickness of the confined PS-*b*-PMMA film, eventually affecting the orientation of the microdomains in the BCP layer. From this point of view, it is necessary to understand how the width of the mesa affects the BCP self-assembly process. Figure 7 reports some SEM images representative of the gratings with

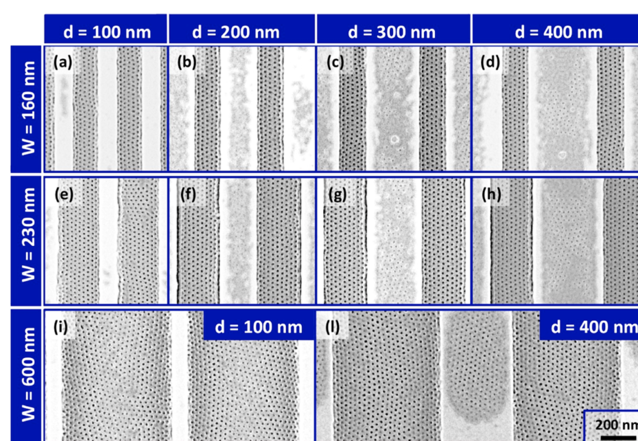

Figure 7. SEM images representing the surface morphology of BCP films treated at T_a of 190 °C and confined inside a periodic structure with mesa width between 100 nm ≤ d ≤ 400 nm and variable trench width (a–d) W = 160 nm (e–f), W = 260 nm, and (i–l) W = 600 nm.

different geometrical parameters annealed at T_a = 190 °C. The microdomains in the confined PS-*b*-PMMA films are perpendicularly oriented with respect to the substrate for all the d values. Interestingly, different amounts of residual polymer are present on the mesa depending on the specific d value. In particular, the mesa regions pertaining to periodic gratings with d = 100 nm are almost completely free of BCP residuals, irrespective of W (Figure 7a,e,i). Conversely, the presence of BCP residuals on the mesa with d = 200, 300, and 400 nm is observed for all the analyzed gratings with W between 130 and 600 nm.

In detail, the AFM images and thickness profiles corresponding to the group of trenches with W = 260 nm but different mesa width values (i.e., d = 100, 200, 300, and 400 nm) are illustrated in Figure 8. For d = 100 nm, the mesa region is empty (Figure 8a). As d increases to 200 nm (Figure 8b), only the mesa regions corresponding to the outer trenches are empty, whereas a substantial amount of BCP is located on the mesa of the central trenches. On further increasing of d to 300

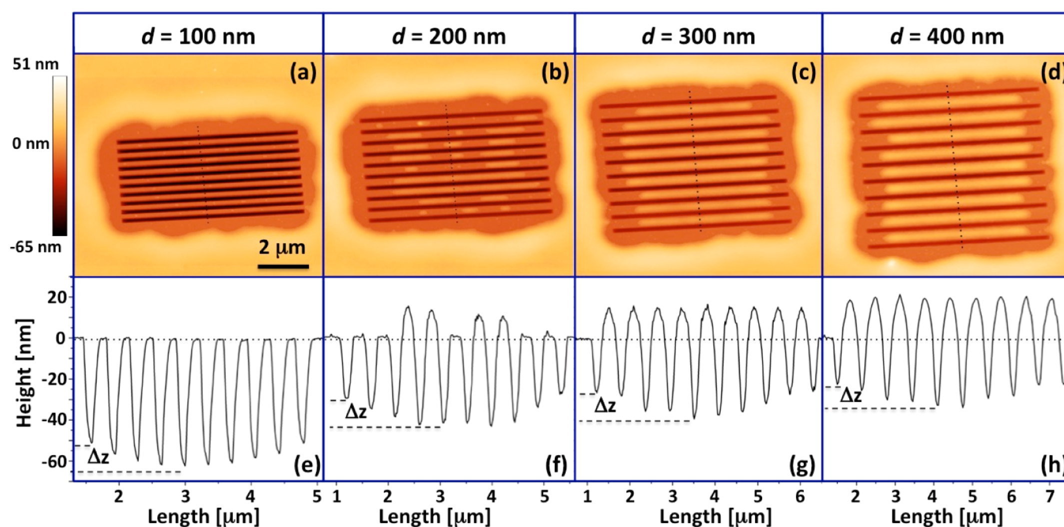

Figure 8. (a−d) AFM micrograph and (e−h) transversal AFM profiles of the periodic grating for a sample treated at T_a = 190 °C with trench width W = 260 nm and variable mesa width 100 nm ≤ d ≤ 400 nm, showing the different thicknesses of the film as a function of the trench position. The dashed lines indicate the thickness difference Δz observed between the more external trench and the central one.

and 400 nm, all the mesa regions are occupied by a BCP layer, as shown in Figure 8c,d. The AFM profiles extracted in the direction perpendicular to the long edge of the trenches (Figure 8e−h) revealed that the amount of BCP confined inside the trenches increases as the width of the mesa region increases. This result indicates that although the mesa regions are not completely empty the amount of BCP that flows from the mesa to the trenches increases as the width of the mesas increases. Furthermore, in all the groups, a different BCP content was detected in the various trenches, depending on the relative position of the trench with respect to the center of the grating. The thickness of the confined BCP is lower inside the central trenches and progressively increases toward the external trenches. Interestingly, such variation of thickness (Δz) between the central and external trenches is fairly constant irrespective of the width of the mesa region. This is related to the disposition of the BCP film over the periodic gratings during the spinning process. The AFM profiles demonstrate that prior to the RTP treatment the BCP film exhibits no evidence of fracture in the region of the gratings. The continuous BCP film assumes a sinusoidal shape over the periodic grating and reported in Figure S3.

Figure 9a shows the AFM profiles acquired in the longitudinal direction of the central trenches with W = 260 nm and different values of d. Similar to Figure 6, to give a significant overview of trench height profile, different horizontal and vertical scales are adopted. Because the trenches are 90 nm deep, the resultant film thicknesses of the central trenches are between h = 30 nm, for the grating with d = 100 nm, and h = 60 nm, for the grating with d = 400 nm, consistent with those of the AFM profiles in Figure 8. The film thickness along the trench is quite constant.

These results point out that the mesa acts as a BCP reservoir that empties during the annealing treatment. Combination of the AFM images and profiles indicate the presence of a polymeric film of uniform thickness within each trench, but significant variations of thickness are observed as a function of the position of the trench within the periodic grating and of the mesa width. From a technological point of view, this is an interesting result because the geometrical parameters of the grating strongly affect the BCP thickness inside the trenches and consequently the aspect ratio (AR) of the cylinders in the polymeric mask. The cylinder AR values corresponding to the central trenches (black squares) and lateral trenches (red dots) as a function of d are illustrated in Figure 9b, which takes into consideration that the cylinders have a diameter of 13 nm. AR in the central trenches ranges from 2.3 for d = 100 nm to 4.2 for d = 400 nm, and the AR further increases in the external trenches, up to values of ∼5.5, thus indicating a substantial spreading of the ARs. However, despite this AR variation, the confined BCP films self-assemble in hexagonally packed PMMA cylinders within the PS matrix, preserving the perpendicular orientation of the microdomains with respect to the substrate, irrespective of the geometrical constrains. This intrinsic robustness of the process represents an important output of this study because it provides a high level of flexibility in the design of the topographically defined pattern that is used to register the BCP template with the underlying substrate.

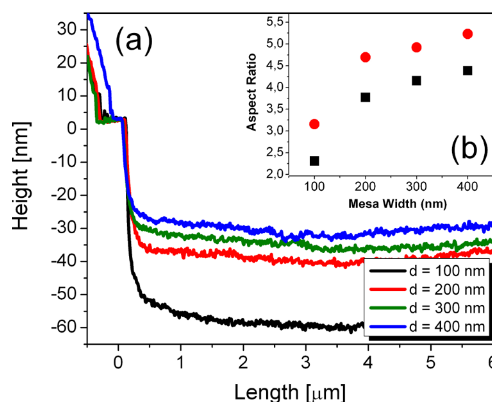

Figure 9. (a) Longitudinal AFM profiles inside central trenches with the same width W = 260 nm and different mesa widths 100 nm ≤ d ≤ 400 nm. (b) Aspect ratio of the confined BCP film calculated for the central trench (black squares) and the external trench (red dots) as a function of d.

CONCLUSIONS

Extensive investigation was reported about the confinement and ordering process of cylinder forming PS-*b*-PMMA BCP thin film within periodic structures, composed by several topographically defined trenches within a SiO_2 matrix. The flow of polymer from the flat areas adjacent to the trenches was studied in detail, showing a variation of the thickness of the confined polymeric film as a function of the processing temperature (180−230 °C) and of the geometrical parameters, i.e., the width of the trenches and the distance between the trenches within the periodic structure. The thickness variation of the BCP film in the trenches strongly affects the ordering process, ultimately leading to different orientation of the microdomains within the trenches. Processing the samples at 230 and 210 °C, a mixed morphology is observed within the trenches with the appearance of either a multidomain structure with parallel and perpendicular cylinders coexisting along the trench or a peculiar morphology with a central zone of perpendicular cylinders and two lateral areas symmetrically placed relative to the central zone featuring cylinders in the parallel orientation to the substrate surface and in the perpendicular oriented with respect to the long side of the trench walls. Conversely, on annealing the samples at 190 °C for 900 s, a precise confinement of the BCP film within the trenches is observed, with a perpendicular orientation of the microdomains irrespective of the trench width and distance. Further lowering the annealing temperature (T_a = 180 °C) results in a continuous polymeric film with no confinement of the BCP within the trenches. The combination of these effects results in a narrow window of temperatures for the processing of this PS-*b*-PMMA BCP. However, operating at 190 °C, the intrinsic robustness of the self-assembly process guarantees the possibility to design the topographically defined template in the SiO_2 without any detrimental effect on the final arrangement of the BCP within the guiding structures.

ASSOCIATED CONTENT

Supporting Information

The Supporting Information is available free of charge on the ACS Publications website at DOI: 10.1021/acsami.5b07127.

AFM top view and height profiles of pristine template, RCP-functionalized surface after the RTP treatment, periodic grating covered by the BCP before the thermal treatment, and the rims created at the annealing temperature of T_a = 230 °C. (PDF)

AUTHOR INFORMATION

Corresponding Author

*E-mail: federico.ferrareselupi@mdm.imm.cnr.it.

Notes

The authors declare no competing financial interest.

ACKNOWLEDGMENTS

This research has been financially supported by the European Metrology Research Programme (EMRP), Project SiB61 CRYSTAL. The EMRP is jointly funded by the EMRP participating countries within EURAMET and the European Union. Partial financial support by PRIN 2010-2014 Materiali Polimerici Nanostrutturati con Strutture Molecolari e Crystalline Mirate is acknowledged. Patent protection related to this work is pending (International Patent Application No. PCT/IB2014/061324).

REFERENCES

(1) *International Technology Roadmap for Semiconductors: Emerging Research Materials*, 2011. http://www.itrs.net/reports.html.

(2) Darling, S. B. B. Directing the Self-Assembly of Block Copolymers. *Prog. Polym. Sci.* **2007**, *32* (10), 1152−1204.

(3) Bang, J.; Jeong, U.; Ryu, D. Y.; Russell, T. P.; Hawker, C. J. Block Copolymer Nanolithography: Translation of Molecular Level Control to Nanoscale Patterns. *Adv. Mater.* **2009**, *21* (47), 4769−4792.

(4) Ouk Kim, S.; Solak, H. H.; Stoykovich, M. P.; Ferrier, N. J.; de Pablo, J. J.; Nealey, P. F. Epitaxial Self-Assembly of Block Copolymers on Lithographically Defined Nanopatterned Substrates. *Nature* **2003**, *424* (6947), 411−414.

(5) Liu, G.; Detcheverry, F.; Ramirez-Hernandez, A.; Yoshida, H.; Tada, Y.; de Pablo, J. J.; Nealey, P. F. Nonbulk Complex Structures in Thin Films of Symmetric Block Copolymers on Chemically Nanopatterned Surfaces. *Macromolecules* **2012**, *45*, 3986−3992.

(6) Jeong, S.-J.; Kim, J. E.; Moon, H.-S.; Kim, B. H.; Kim, S. M.; Kim, J. B.; Kim, S. O. Soft Graphoepitaxy of Block Copolymer Assembly with Disposable Photoresist Confinement. *Nano Lett.* **2009**, *9* (6), 2300−2305.

(7) Jeong, S.-J.; Kim, S. O. Ultralarge-Area Block Copolymer Lithography via Soft Graphoepitaxy. *J. Mater. Chem.* **2011**, *21* (16), 5856−5859.

(8) Park, S.-M.; Rettner, C. T.; Pitera, J. W.; Kim, H.-C. Directed Self-Assembly of Lamellar Microdomains of Block Copolymers Using Topographic Guiding Patterns. *Macromolecules* **2009**, *42* (15), 5895−5899.

(9) Sundrani, D.; Darling, S. B.; Sibener, S. J. Guiding Polymers to Perfection: Macroscopic Alignment of Nanoscale Domains. *Nano Lett.* **2004**, *4* (2), 273−276.

(10) Welander, A. M.; Nealey, P. F.; Cao, H.; Bristol, R. Impact of Trench Width Roughness on the Graphoepitaxial Assembly of Block Copolymers. *J. Vac. Sci. Technol. B Microelectron. Nanom. Struct.–Process., Meas., Phenom.* **2008**, *26* (6), 2484−2488.

(11) Perego, M.; Andreozzi, A.; Vellei, A.; Ferrarese Lupi, F.; Seguini, G. Collective Behavior of Block Copolymer Thin Films within Periodic Topographical Structures. *Nanotechnology* **2013**, *24* (24), 245301.

(12) Aissou, K.; Mumtaz, M.; Fleury, G.; Portale, G.; Navarro, C.; Cloutet, E.; Brochon, C.; Ross, C. a.; Hadziioannou, G. Sub-10 Nm Features Obtained from Directed Self-Assembly of Semicrystalline Polycarbosilane-Based Block Copolymer Thin Films. *Adv. Mater.* **2015**, *27* (2), 261−265.

(13) Segalman, R. a.; Yokoyama, H.; Kramer, E. J. Graphoepitaxy of Spherical Domain Block Copolymer Films. *Adv. Mater.* **2001**, *13* (15), 1152−1155.

(14) Ilievski, F.; Ross, C. a. Graphoepitaxy of Block Copolymers Using Selectively Removable Templates. *J. Vac. Sci. Technol. B Microelectron. Nanom. Struct.–Process., Meas., Phenom.* **2010**, *28* (1), 42−44.

(15) Cheng, J. Y.; Mayes, A. M.; Ross, C. a. Nanostructure Engineering by Templated Self-Assembly of Block Copolymers. *Nat. Mater.* **2004**, *3* (11), 823−828.

(16) Tong, Q.; Sibener, S. J. Visualization of Individual Defect Mobility and Annihilation within Cylinder-Forming Diblock Copolymer Thin Films on Nanopatterned Substrates. *Macromolecules* **2013**, *46* (21), 8538−8544.

(17) Park, S.-M.; Stoykovich, M. P.; Ruiz, R.; Zhang, Y.; Black, C. T.; Nealey, P. F. Directed Assembly of Lamellae- Forming Block Copolymers by Using Chemically and Topographically Patterned Substrates. *Adv. Mater.* **2007**, *19* (4), 607−611.

(18) Maher, M. J.; Rettner, C. T.; Bates, C. M.; Blachut, G.; Carlson, M. C.; Durand, W. J.; Ellison, C. J.; Sanders, D. P.; Cheng, J. Y.; Willson, C. G. Directed Self-Assembly of Silicon-Containing Block Copolymer Thin Films. *ACS Appl. Mater. Interfaces* **2015**, *7* (5), 3323−3328.

(19) Han, E.; Kang, H.; Liu, C.-C.; Nealey, P. F.; Gopalan, P. Graphoepitaxial Assembly of Symmetric Block Copolymers on Weakly Preferential Substrates. *Adv. Mater.* **2010**, *22* (38), 4325−4329.

(20) Koh, H.-D.; Park, Y. J.; Jeong, S.-J.; Kwon, Y.-N.; Han, I. T.; Kim, M.-J. Location-Controlled Parallel and Vertical Orientation by Dewetting-Induced Block Copolymer Directed Self-Assembly. *J. Mater. Chem. C* **2013**, *1* (25), 4020−4024.

(21) Kim, S.; Shin, D. O.; Choi, D. G.; Jeong, J. R.; Mun, J. H.; Yang, Y. B.; Kim, J. U.; Kim, S. O.; Jeong, J. H. Graphoepitaxy of Block-Copolymer Self-Assembly Integrated with Single-Step ZnO Nano-imprinting. *Small* **2012**, *8* (10), 1563−1569.

(22) Mokarian-Tabari, P.; Collins, T. W.; Holmes, J. D.; Morris, M. A. Cyclical "Flipping" of Morphology in Block Copolymer Thin Films. *ACS Nano* **2011**, *5* (6), 4617−4623.

(23) Ferrarese Lupi, F.; Giammaria, T. J.; Seguini, G.; Laus, M.; Enrico, E.; De Leo, N.; Boarino, L.; Ober, C. K.; Perego, M. Thermally Induced Orientational Flipping of Cylindrical Phase Diblock Copolymers. *J. Mater. Chem. C* **2014**, *2* (12), 2175−2182.

(24) Sparnacci, K.; Antonioli, D.; Gianotti, V.; Laus, M.; Ferrarese Lupi, F.; Giammaria, T. J.; Seguini, G.; Perego, M. Ultrathin Random Copolymer-Grafted Layers for Block Copolymer Self-Assembly. *ACS Appl. Mater. Interfaces* **2015**, *7*, 10944−10951.

(25) Russell, T. P.; Hjelm, R. P.; Seeger, P. A. Temperature Dependence of the Interaction Parameter of Polystyrene and Poly (methyl methacrylate). *Macromolecules* **1990**, *23*, 890−893.

(26) Ferrarese Lupi, F.; Giammaria, T. J.; Seguini, G.; Vita, F.; Francescangeli, O.; Sparnacci, K.; Antonioli, D.; Gianotti, V.; Laus, M.; Perego, M. Fine Tuning of Lithographic Masks through Thin Films of PS-B-PMMA with Different Molar Mass by Rapid Thermal Processing. *ACS Appl. Mater. Interfaces* **2014**, *6*, 7180−7188.

(27) Ferrarese Lupi, F.; Giammaria, T. J.; Ceresoli, M.; Seguini, G.; Sparnacci, K.; Antonioli, D.; Gianotti, V.; Laus, M.; Perego, M. Rapid Thermal Processing of Self-Assembling Block Copolymer Thin Films. *Nanotechnology* **2013**, *24* (31), 315601.

(28) Ceresoli, M.; Ferrarese Lupi, F.; Seguini, G.; Sparnacci, K.; Gianotti, V.; Antonioli, D.; Laus, M.; Boarino, L.; Perego, M. Evolution of Lateral Ordering in Symmetric Block Copolymer Thin Films upon Rapid Thermal Processing. *Nanotechnology* **2014**, *25* (27), 275601.

(29) Harrison, C.; Angelescu, D. E.; Trawick, M.; Cheng, Z.; Huse, D. a; Chaikin, P. M.; Vega, D. a; Sebastian, J. M.; Register, R. a; Adamson, D. H. Pattern Coarsening in a 2D Hexagonal System. *Europhys. Lett.* **2004**, *67* (5), 800−806.

(30) Ferrarese Lupi, F.; Giammaria, T. J.; Volpe, F. G.; Lotto, F.; Seguini, G.; Pivac, B.; Laus, M.; Perego, M. High Aspect Ratio PS - B - PMMA Block Copolymer Masks for Lithographic Applications. *ACS Appl. Mater. Interfaces* **2014**, *6*, 21389−21396.

(31) Limary, R.; Green, P. F. Dewetting Instabilities in Thin Block Copolymer Films: Nucleation and Growth. *Langmuir* **1999**, *15* (17), 5617−5622.

(32) Masson, J.-L.; Limary, R.; Green, P. F. Pattern Formation and Evolution in Diblock Copolymer Thin Films above the Order−disorder Transition. *J. Chem. Phys.* **2001**, *114* (24), 10963−10967.

DOI: 10.1021/acsami.5b07127
ACS Appl. Mater. Interfaces 2015, 7, 23615−23622